Performance Evaluation of KBH$_4$ as Energy Carrier for Shipping Applications

Andrea Düll, Patrick Rohlfs, Olaf Deutschmann, and Marion Börnhorst*

Non-fossil fuels are urgently needed for maritime and inland shipping applications to mitigate the sector's adverse impact on the global climate. This study investigates the performance of potassium borohydride (KBH$_4$) as an alternative, carbon-free energy carrier on the basis of detailed process simulations of the overall energy storage cycle in Aspen Plus®. After optimizing the individual on-board and off-board process steps, the feasibility of installing a KBH$_4$-based energy supply system on board of an inland-waterway cargo vessel is evaluated and critical process steps are highlighted along with current research challenges.

Keywords: Borohydrides, Fuel cells, Hydrogen storage, Multiphase reactors, Process simulation

Received: October 30, 2021; *revised:* February 22, 2022; *accepted:* March 14, 2022

1 Introduction

Anthropogenic greenhouse gas (GHG) emissions are responsible for continuous global warming [1]. In 2019, the global average temperature reached 1.1 °C above pre-industrial levels and global warming is expected to increase even further; currently by a rate of 0.2 °C per decade [2]. In order to avoid significant and irreversible damage to the natural ecosystem and human society, the global community has agreed on taking measures to limit global warming below 2 °C compared to pre-industrial times during the Paris Climate Conference in 2015 [3]. Such ambitious goals can, however, only be achieved through a significant reduction of GHG emissions from all sectors [1].

Accounting for 25 % of the global carbon dioxide (CO$_2$) emissions, transportation-related activities are a major contributor to climate change [4]. The shipping industry is currently responsible for only 2.64 % of these emissions [5], but under a business-as-usual scenario, shipping emissions are projected to have increased up to 250 % by 2050 due to an increased demand for international sea freight transport [6]. This development jeopardizes the ambitious Paris Agreement goals [6]. In order to mitigate the shipping sector's adverse impact on the global climate, the International Maritime Organization (IMO) is pursuing efforts to reduce GHG emissions related to international shipping by at least 50 % by 2050 compared to 2008 [7]. Next to technological solutions to increase the energy efficiency of ships (optimization of ship design, use of lighter materials, etc.) and operational measures (reduction of voyage speed, optimization of shipping routes, etc.), the use of alternative fuels is a promising option to fulfill these ambitions [7, 8]. This shift towards an increased use of non-fossil fuels for shipping is accelerated by the IMO's decision to decrease the upper limit on sulfur content of ship fuels from 3.5 % to 0.5 % in 2020 in order to reduce the harmful emissions of sulfur oxide and particulate matter [9, 10].

Next to liquefied natural gas, methanol and biofuels, hydrogen (H$_2$) has been identified as a promising alternative to heavy fuel and marine gas oil, which are currently predominantly employed in the shipping sector [9]. While significant progress is being made in the industrial-scale H$_2$ production from renewable energy through water electrolysis [11, 12] and the use of fuel cells (FC) on board of ships [13, 14], the transportation and large-scale storage of H$_2$ remains a major bottleneck for its wide-spread use as fuel in the shipping industry [15, 16].

With a lower heating value LHV_{H_2} of 120 MJ kg^{-1}, H$_2$ exhibits an excellent gravimetric energy density [17]. However, due to the gas's low density at atmospheric conditions, its energy content by volume of 9.9 MJ m^{-3} is not competitive with that of fossil fuels [15, 18]. In response to this challenge, a variety of different storage technologies has been developed. Physical-based storage methods include the storage of pure H$_2$ in compressed, liquefied or cold/cryo-compressed form, while material-based storage technologies rely on the use of storage materials. The latter can bind large amounts of H$_2$ through physical (zeolites, metal organic frameworks, etc.) or chemical sorption (liquid organic hydrogen carriers, ammonia, metal hydrides, etc.) [18].

Andrea Düll, Patrick Rohlfs, Prof. Dr. Olaf Deutschmann, Dr. Marion Börnhorst
marion.boernhorst@kit.edu
Karlsruhe Institute of Technology, Institute for Chemical Technology and Polymer Chemistry, Engesserstraße 20, 76131 Karlsruhe, Germany.

Among the chemical H_2 storage materials, metal borohydrides and in particular sodium borohydride ($NaBH_4$) have received significant attention over the past two decades, as the chemically bound H_2 can be released via hydrolysis under relatively mild conditions [19]. Continuous research efforts have, however, not yet resulted in the H_2 storage material's successful commercialization but have, in contrast, suffered serious setbacks [20]. From an engineering point of view, the successful implementation in technical systems is mainly complicated by the limited solubility of the hydrolysis by-product sodium metaborate ($NaBO_2$), which entails the risk for by-product accumulation within the H_2 release reactor and eventual system clogging [21].

The present study focuses on a rather similar alkali borohydride for use as H_2 storage material in the shipping sector: potassium borohydride (KBH_4). Due to its higher molar mass and therefore lower theoretical gravimetric H_2 storage capacity compared to $NaBH_4$, KBH_4 has been much less investigated [19] apart from isolated studies regarding material properties [22–25], the hydrolysis reaction [26–30] as well as a series of patents [31–34]. However, KBH_4 is less hygroscopic than $NaBH_4$ [35, 36], less heat is released during the hydrolysis reaction [35] and the hydrolysis by-product potassium metaborate (KBO_2) is much less susceptible to crystallization than $NaBO_2$ at low system temperatures [22–25].

In this contribution, the potential of KBH_4 as energy carrier in the shipping sector is evaluated on the basis of a detailed analysis of the full KBH_4-based energy storage cycle. While alkali borohydrides have previously mainly been considered for application on board of light-duty vehicles or for use in portable devices [37], this study focuses on the application of KBH_4 in the shipping industry, not only due to the vast potential for reduction of GHG emissions in this sector [6], but also due to the nature of the on-board H_2 release: H_2 is released from KBH_4 through hydrolysis, i.e., through the reaction between KBH_4 and water (H_2O). In case of shipping applications, the latter can be directly extracted from the waters surrounding the vessel, thereby eliminating the need for storing large amounts of H_2O on board, which directly increases the carrier's overall energy storage capacity [38].

2 Modeling Framework

The following section describes the modeling strategy followed in the present study.

2.1 Process Overview

The envisaged KBH_4-based fuel cycle, which serves as the basis for the present study, can be divided into two locally separated subprocesses, as depicted in Fig. 1. On board of the inland waterway or seagoing vessel, the energy carrier, which is stored in the form of a dry, solid powder to avoid spontaneous H_2 liberation through self-hydrolysis [26], is mixed with H_2O. The latter can either be stored in a separate tank or directly produced on board of the ship from the waters surrounding the vessel through reverse osmosis. While the use of such a reverse osmosis system has also been considered in a recently published feasibility study regarding the use of $NaBH_4$ as H_2 storage material for inland shipping applications [39], such costly water purification might not be necessary and, depending on the water quality, seawater could be directly used in the hydrolysis reaction as exemplarily demonstrated by Xi et al. [40] in the case of $NaBH_4$.

The resulting aqueous mixture is preheated and fed to a catalytic reactor, where H_2 is generated through hydrolysis. The latter is fed to a proton-exchange membrane fuel cell (PEMFC), while the H_2-lean, aqueous by-product solution is stored on board of the ship until it can be unloaded at a designated harbor and brought to a regeneration facility. There, it needs to be dried and regenerated.

A variety of different methods have been proposed for the rehydrogenation of $NaBO_2$ during the last two decades, as summarized in a detailed review by Nunes et al. [41]. According to the type of energy source, these processes can
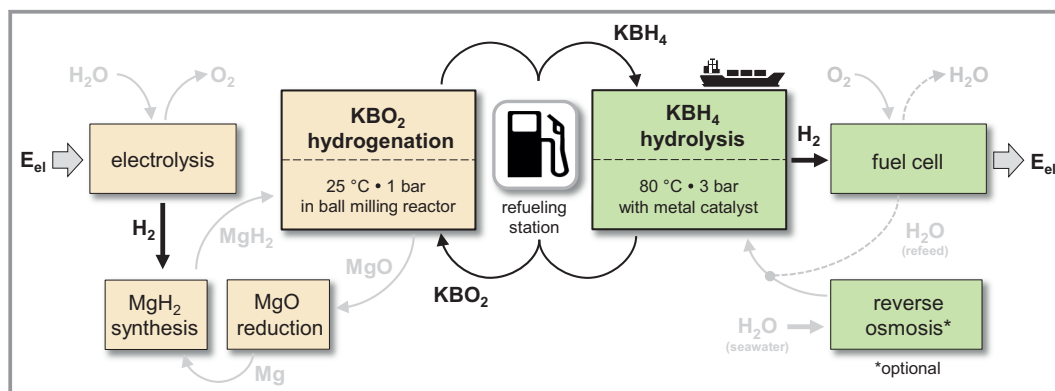

Figure 1. KBH_4-based energy storage cycle for shipping applications; only major process steps and streams shown for reasons of clarity.

be grouped into electrochemical, thermochemical and mechanochemical regeneration pathways, of which the mechanochemical reduction of $NaBH_4$ in the presence of an auxiliary metal is currently the most advanced [41, 42]. The regeneration of KBH_4 has been much less explored. The few reported regeneration methods are, however, similar to the ones proposed for $NaBH_4$ [32, 43]. The regeneration scheme adapted in the present study is based on a study by Li et al. [43], who demonstrated that KBH_4 can be mechanochemically synthesized from anhydrous KBO_2 through ball milling with magnesium hydride (MgH_2) under ambient conditions. Full conversion of KBO_2 was reported to be achieved in case MgH_2 was supplied in excess to the reactant mixture [43].

The supplied MgH_2 is oxidized in the course of the regeneration process. Thus, in order to achieve a fully closed fuel cycle, the reduction of the generated magnesium oxide (MgO) as well as the rehydrogenation of the as-produced magnesium (Mg) is indispensable, which greatly increases the complexity of the overall system.

2.2 Aspen Plus® Process Model Setup and Simulation Strategy

The process simulation software Aspen Plus® V12 [44] was used to simulate the previously described energy storage cycle on the basis of mass and energy balances without considering the kinetics of the involved process steps or process economics. Customized models were integrated into the simulation environment by dynamically linking Aspen Plus® to Microsoft® Excel.

As most physical properties of the storage cycle's two key components KBH_4 and KBO_2 are not available in the software's standard material property database, the missing parameters were either supplied from external data bases such as the NIST Chemistry WebBook [45, 46] or regressed with the software's built-in data regression system. In particular, the temperature-dependent solubility was modeled using an electrolyte non-random-two-liquid (ELECNRTL [47]) model under the assumption of negligible pressure dependence. The necessary input values, namely equilibrium and binary interaction parameters, were determined based on experimental data from literature [22–24]. Exemplarily, the determined solubility curve of KBO_2 in H_2O along with the corresponding reference literature data is shown in Fig. 2. As can be taken from the figure, the solubility of KBO_2 in H_2O is only slightly dependent on temperature. In contrast, the solubility of $NaBO_2$ in H_2O exhibits a much more pronounced temperature dependence with solubilities ranging from 16 wt % at 5 °C to 49 wt % at 95 °C [48].

The modeling of the on-board KBH_4 hydrolysis and of the onshore KBH_4 synthesis as well as of the onshore Mg regeneration and MgH_2 synthesis is presented in the following.
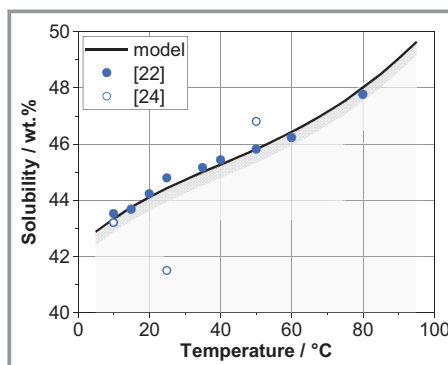

Figure 2. Solubility of KBO_2 in H_2O as a function of temperature; region, in which KBO_2 and H_2O form homogeneous mixtures is indicated in light gray, and region of interest for hydrolysis by-product composition is qualitatively highlighted by a hatching.

2.2.1 On-board Hydrogen Release

H_2 is released on board of the ship through the hydrolysis of KBH_4. This reaction proceeds spontaneously upon contact of KBH_4 with H_2O in dependence on the system temperature and the composition of the aqueous reactant mixture. However, it is generally carried out in the presence of a metal catalyst to accelerate the H_2 release process [26, 28]. While catalysts based on noble metals such as rhodium, ruthenium and platinum exhibit superior catalyst activities and stabilities, the use of non-noble metals such as cobalt has been of continuous interest in view of the raw material's lower price [49].

The hydrolysis reaction temperatures and pressures are in excellent agreement with the typical operating conditions of common low-temperature PEMFCs. The latter usually operate at temperatures T between 50 and 80 °C and pressures p between 1 and 3 bar [50]. In case of sufficiently high H_2O/KBH_4 feed ratios (FR) for full dissolution of the hydrolysis by-product, the hydrolysis reaction can be represented by Eq. (1) [19, 22, 51]:

$$KBH_4 + (4 + n_{ex})H_2O \rightarrow KB(OH)_4 + 4H_2 + n_{ex}H_2O$$
$$\Delta H_R < 0 \tag{1}$$
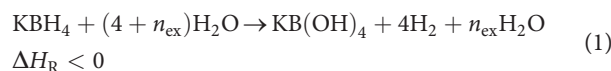
Here, it should be noted that a potassium tetrahydroxyborate rather than a potassium metaborate solution is generated during hydrolysis with the formed metaborate ions being present in the aqueous solution in the form of $B(OH)_4^-$ [51].

According to the previously presented reaction equation, H_2O not only serves as a reactant, which supplies half of the generated H_2, but also as a solvent for the hydrolysis by-product, as is the case with the hydrolysis of $NaBH_4$ [19]. Thus, H_2O must be fed in excess amounts n_{ex} to the reactor to avoid the formation of super-saturated, aqueous solutions and thereby reduce the risk for by-product crystallization and reactor clogging. This additional H_2O supply must, however, be kept as low as possible to save weight on

board of the ship. The resulting region of interest for the hydrolysis by-product composition is qualitatively highlighted in the corresponding solubility diagram in Fig. 2 by a hatching.

The process flow sheet of the on-board H_2 release through hydrolysis of KBH_4, which served as basis for the Aspen Plus® simulations is depicted in Fig. 3. The corresponding major unit operations are specified in Tab. 1. In the process flow diagrams in Fig. 3 as well as in the following Fig. 4 and Fig. 5, energy streams that were considered for the calculation of the overall energy efficiency are indicated by dashed arrows. Furthermore, the legend given in Fig. 3 is also applicable to the process flow diagrams in Fig. 4 and Fig. 5.

The following major assumptions were considered in the model:

– All process steps are at steady state.
– The reactant feed streams consist of 100 % KBH_4 or H_2O. This assumption serves as mere simplification for modeling purposes, while in reality, impurities would be present in the supplied raw materials.
– The hydrolysis reaction (R1) proceeds with a KBH_4 conversion X of 100 % [32].
– Electricity is generated in the FC (HyPM™ HD 180, Hydrogenics) with an efficiency η_{FC} in the range of 40–55 % and an efficiency η_{FC} of approx. 50 % under half load according to this FC's typical performance curve [52].
– Heat losses to the environment as well as the power consumption of auxiliary system components are neglected.

Furthermore, the process simulation is based on the following design specifications:

– The KBH_4 feed flow rate is adapted according to the required FC power output and corresponding H_2 demand.
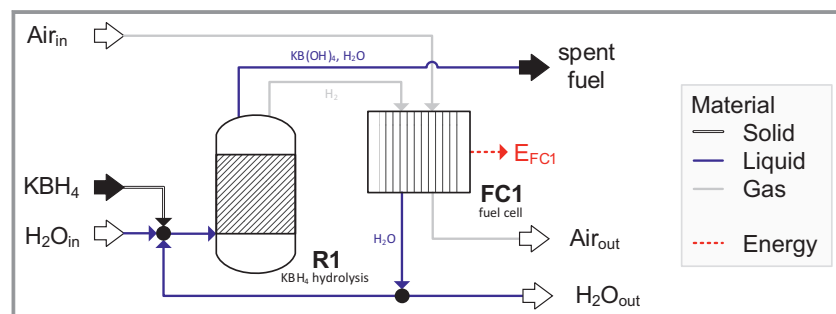
– The H_2O feed is set to the minimum possible flow rate, at which by-product crystallization within the reactor is avoided.
– The air supply to the FC is adapted according to the H_2 feed stream to achieve a stoichiometric H_2/O_2 mixture.

2.2.2 Onshore Potassium Borohydride Regeneration

As briefly described in Sect. 2.1, the present study assumes the synthesis of KBH_4 through rehydrogenation of KBO_2 in the presence of MgH_2 in a ball milling reactor under ambient conditions. As a low H_2O content in the reactant mixture was found to be crucial for achieving high KBH_4 yields [43], the residual H_2O must be fully removed from the spent fuel beforehand. The synthesis of KBH_4 from anhydrous KBO_2 and MgH_2 can be represented by [43]:

$$KBO_2 + 2\,MgH_2 \rightarrow KBH_4 + 2\,MgO \quad \Delta H_R < 0 \quad (2)$$
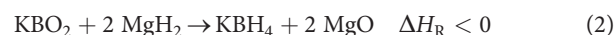
For separation of the solid reaction products, the present study considers the solvent extraction of KBH_4 with ethylenediamine (EDA) and the subsequent solvent regeneration through thermal evaporation.

The process flow sheet of the onshore KBH_4 regeneration, which served as basis for the Aspen Plus® simulations, is depicted in Fig. 4. The corresponding major unit operations are specified in Tab. 2.

The following major assumptions were considered in the model:

– All process steps are at steady state.
– Anhydrous KBO_2 can be obtained by removal of H_2O from the spent fuel solution (E1) at temperatures above 250 °C [53].
– KBO_2 is fully converted to KBH_4 in the KBH_4 synthesis reactor (R2) [43].

– During product extraction (S1), KBH_4 is dissolved in EDA up to molar KBH_4 contents $x_{KBH_4,L}$ of 0.0417.
– 20 % of the EDA supplied to the product extraction step (S1) remains in the solid phase.
– Heat losses to the environment as well as the power consumption of auxiliary system components are neglected. In particular, the necessary input of mechanical energy during ball milling (R2) is not considered in the present study due to a lack of literature data regarding the performance and power

Figure 3. Process flow sheet of the on-board hydrolysis of KBH_4, which served as basis for the Aspen Plus® simulations.
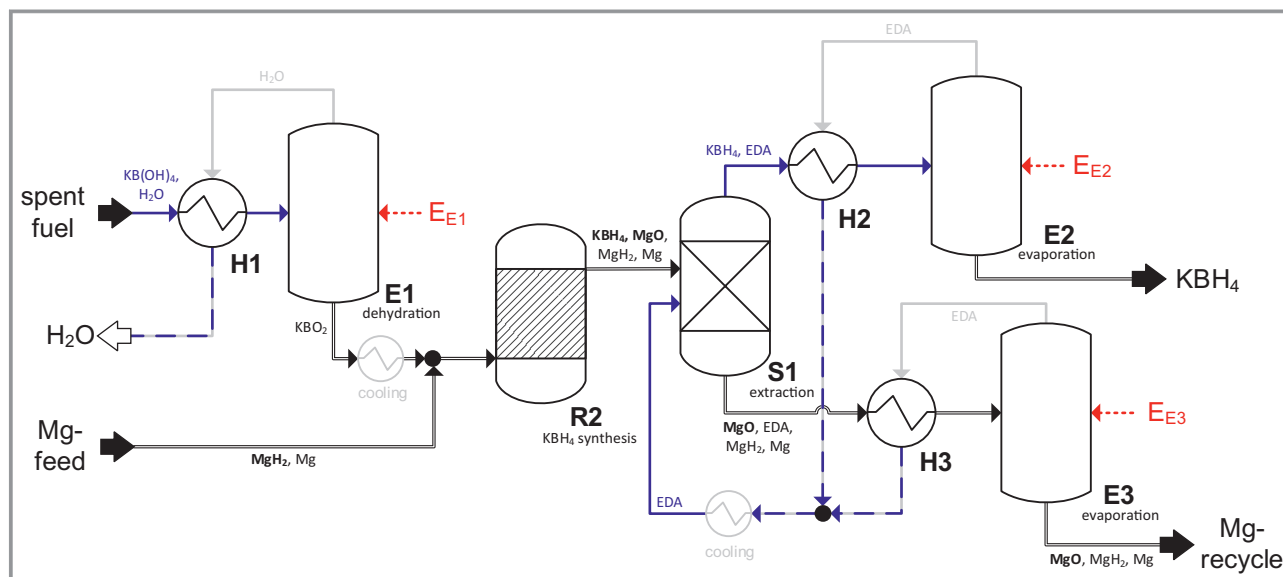
Table 1. Description of the major Aspen Plus® unit operations (UO) employed for modeling the on-board hydrolysis of KBH_4.

UO	T [°C]	p [bar]	Model	Specifications
R1	80	3	RStoic	$KBH_4 + (4 + n_{ex})\,H_2O \rightarrow KB(OH)_4 + 4\,H_2 + n_{ex}\,H_2O,\ X = 1$
FC1 (a)	80	3	RGibbs	$H_2 + 0.5\,O_2 \rightarrow H_2O,\ X = 1$
FC1 (b)	–	–	Calculator	$E_{FC1} = |\Delta H_R|\eta_{FC}$

www.cit-journal.com

© 2022 The Authors. Chemie Ingenieur Technik published by Wiley-VCH GmbH

Chem. Ing. Tech. **2022**, *94*, No. 5, 1–14

Figure 4. Process flow sheet of the onshore KBH$_4$ regeneration, which served as basis for the Aspen Plus® simulations.

Table 2. Description of the major Aspen Plus® unit operations (UO) employed for modeling the onshore KBH$_4$ regeneration.

UO	T [°C]	p [bar]	Model	Specifications
E1	250	1	Flash2	$x_{H_2O,S} = 0$
R2	25	1	Rstoic	$KBO_2 + 2\,MgH_2 \rightarrow KBH_4 + 2\,MgO$, $X = 1$
S1	25	1	Sep	$x_{KBH_4,L} = 0.047$, $x_{EDA,L} = 0.953$
E2 / E3	120	1	Flash2	$x_{EDA,S} = 0$
H1	100 ($T_{max,cold}$)	1	HeatX	$T_{out,cold} = 100\,°C$
H2 / H3	110 ($T_{max,cold}$)	1	HeatX	$\Delta T_{min} = 10\,°C$

consumption of an upscaled ball milling reactor for KBH$_4$ synthesis.

Furthermore, the process simulation is based on the following design specifications:

– The MgH$_2$ supply to the KBH$_4$ synthesis reactor (R2) is adjusted according to the KBO$_2$ feed stream in a way that the reactant mixture contains 2.7 mol$_{MgH2}$ mol$_{KBO2}$$^{-1}$ [43].
– The EDA supply is set to the minimum flow rate, which allows for full KBH$_4$ extraction.
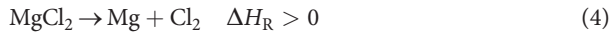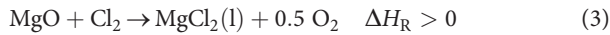
2.2.3 Onshore Magnesium Regeneration and Rehydrogenation

As the continuous generation of waste products during the regeneration of KBH$_4$ needs to be avoided, the reduction of MgO as well as the rehydrogenation of the as-produced Mg must be considered. The metal oxide reduction pathways proposed in literature for closing the NaBH$_4$-based fuel cycle are based on conventional methods for the industrial-scale production of Mg. They include the regeneration of MgO through silicothermic reduction as

applied in the widely used Pidgeon process [54, 55] as well as the production of Mg through molten salt electrolysis of magnesium chloride (MgCl$_2$) [56, 57]. While both production processes, but in particular the former, are characterized by a high energy demand and carbon footprint [58–60], continuous research is being conducted to reduce the process's energy intensity and environmental impact [61, 62] or to derive novel, less energy-intensive pathways for Mg production [63]. The present study considers the regeneration of Mg from MgO through the electrochemical pathway, as the environmental impact of such a process can be significantly decreased through integration of renewable energy sources [59] and a considerable expansion of the latter can be expected within the next years [1].

This method includes the chlorination of MgO at an elevated temperature of 900 °C and the subsequent electrolysis of the generated MgCl$_2$ at 670 °C [56, 61], as represented by Eqs. (3) and (4), respectively. It must be noted that the use of a reducing agent such as carbon for binding the generated oxygen (O$_2$) is necessary for MgO chlorination on an

industrial scale in order to minimize the oxidation of $MgCl_2$ [64]. This is, however, not considered in the present study.

$$MgO + Cl_2 \rightarrow MgCl_2(l) + 0.5\,O_2 \quad \Delta H_R > 0 \tag{3}$$

$$MgCl_2 \rightarrow Mg + Cl_2 \quad \Delta H_R > 0 \tag{4}$$

While heating the MgO-rich material stream generated during KBH_4 synthesis to the elevated operating temperature of the previously described process steps, H_2 is desorbed from the contained residual MgH_2. In the developed process model, this dehydrogenation step is assumed to occur at a constant temperature level and H_2 is assumed to be fully desorbed at a temperature of 450 °C, which represents a simplification in comparison to the experimentally observed desorption behavior [65, 66]. Furthermore, the present study considers the separation of residual Mg from MgO through thermal evaporation of the former prior to the chlorination of the metal oxide.

In order to close the KBH_4-based fuel cycle, Mg generated according to Eqs. (3) and (4) needs to be reacted with H_2 to

form MgH_2 according to Eq. (5) [56] and the generated metal hydride can subsequently be refed to the KBH_4 synthesis reactor.

$$Mg + H_2 \rightarrow MgH_2 \quad \Delta H_R < 0 \tag{5}$$

The process flow sheet of the onshore Mg regeneration and rehydrogenation, which served as basis for the Aspen Plus® simulations is depicted in Fig. 5. The corresponding major unit operations are specified in Tab. 3.

As can be taken from Fig. 5, the electrolysis of H_2O and $MgCl_2$ were included into the model in the form of blackbox processes, for which a specified energy consumption

Table 3. Description of the major Aspen Plus® unit operations (UO) employed for modeling the onshore Mg regeneration and rehydrogenation.

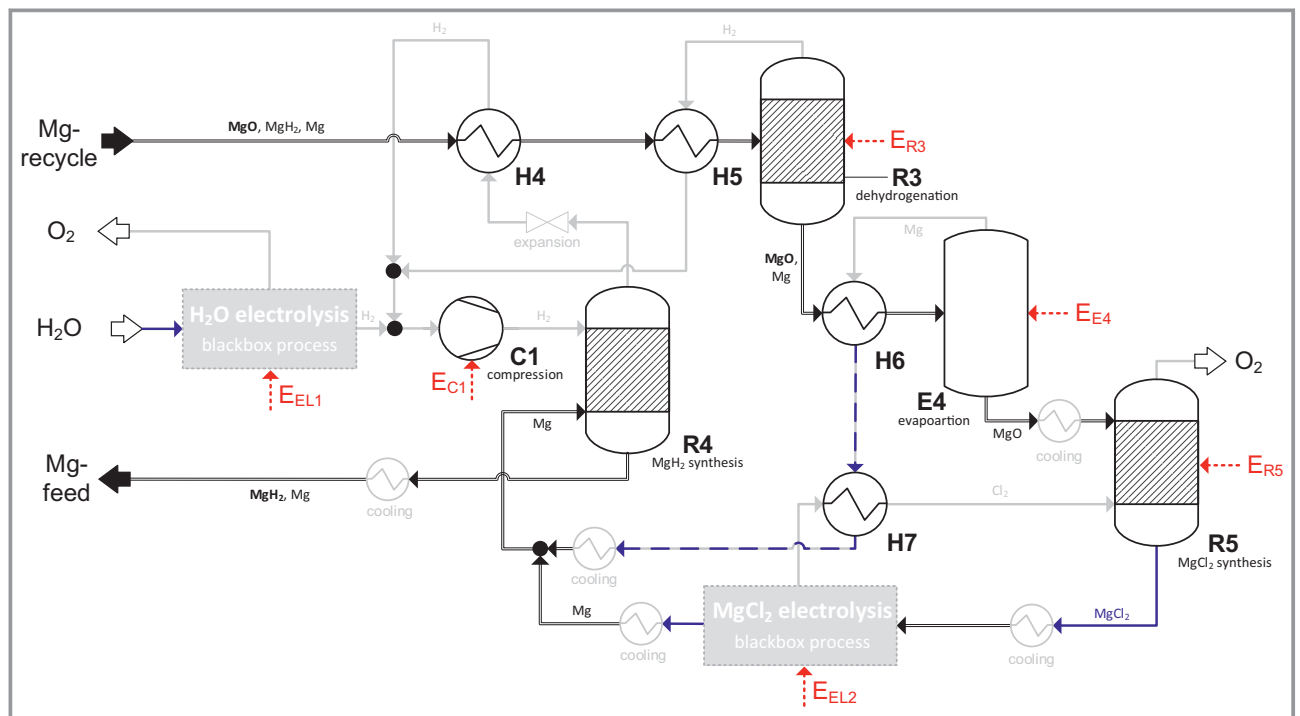| UO	T [°C]	p [bar]	Model	Specifications
R3	450	1	RStoic	$MgH_2 \rightarrow Mg + H_2$, $X = 1$
R4	320	30	RStoic	$Mg + H_2 \rightarrow MgH_2$, $X = 0.9$
R5	900	1	User2	$MgO + Cl_2 \rightarrow MgCl_2 + 0.5\,O_2$, $X = 1$
E4	1093	1	User2	$x_{Mg,S} = 0$
C1	64/270 (in/out)	1/30 (in/out)	Compr	$\eta_{isentropic} = 0.85$, $\eta_{mechanical} = 0.95$
H4 / H5	134 / 183 ($T_{max,cold}$)	1	Heater	$\Delta T_{min} = 10\,°C$
H6 / H7	1080 / 900 ($T_{max,cold}$)	1	User2	$T_{out,cold} = 1080\,°C$ / $900\,°C$

Figure 5. Process flow sheet of the onshore Mg regeneration and rehydrogenation, which served as basis for the Aspen Plus® simulations.

per unit of product was assumed without detailed consideration of the involved process steps. H_2 was assumed to be produced through alkaline water electrolysis with an efficiency of 60 % and a corresponding energy demand E_{EL1} of 198 MJ per kg of H_2 [15]. The energy demand of electrolytic cells for Mg production is dependent on the employed process and the individual production plants [67]. Typical values for industrial processes range from 36 to 47.52 $MJ\,kg_{Mg}^{-1}$ [61, 67, 68], while the energy consumption could be decreased to as low as 28.8 $MJ\,kg_{Mg}^{-1}$ in laboratory experiments [61]. In the present study, an energy demand E_{EL2} of 36 $MJ\,kg_{Mg}^{-1}$ is assumed.

The following major assumptions were considered in the model:

– All process steps are at steady state.
– H_2 compression from 1 to 30 bar (C1) is carried out in two stages with pressure ratios of 7 and 4.3 and intercooling to the initial temperature.
– Mg hydrogenation (R4) proceeds with a Mg conversion X of 90 % [66].
– MgH_2 is fully dehydrogenated at a temperature of 450 °C (R3).
– MgO chlorination (R5) proceeds with a MgO conversion X of 100 %.
– Heat losses to the environment as well as the power consumption of auxiliary system components are neglected.

Furthermore, the process simulation is based on the following design specifications:

– The H_2 supply to the MgH_2 synthesis reactor (R4) is adapted according to the Mg feed stream to achieve a stoichiometric H_2/Mg mixture.
– Similarly, the Cl_2 supply to the $MgCl_2$ synthesis reactor (R5) is adjusted to the MgO feed stream according to the reaction stoichiometry.

2.3 Application Case

As an application case, this study considers a mid-sized inland cargo vessel from Sendo Shipping B.V. [69], which is propelled by two electric motors (Volvo Penta D16) of 450 kW each [70]. While the necessary electricity is currently provided by two diesel generators, the present study assumes the use of five 180 kW PEMFCs (HyPM™ HD 180 [52]) to cater for power demands up to peak loads of 900 kW. Relevant technical specifications can be taken from Tab. 4 and are defined in accordance with literature data [70, 71].

Table 4. Technical specifications of the model ship considered in the present study.

Parameter	Value
Dimensions	110 m × 11.45 m (length × width)
Power demand	450 kW (partial load), 900 kW (full load)
Cargo capacity	164 TEU (3400 t, 6276 m³)

3 Results and Discussion

The developed Aspen Plus® simulation model was employed to optimize and evaluate the individual process steps as well as the overall energy storage cycle as a whole. The results are discussed in the following.

3.1 Optimization of Operating Conditions for On-board Hydrogen Release

The hydrolysis system's overall performance is highly sensitive to the operating temperature, pressure and H_2O/KBH_4 FR. While the operating conditions of the two main system components, i.e., hydrolysis reactor and FC, could theoretically be decoupled through integration of additional temperature and H_2O management systems, the present study assumes hydrolysis reactor and FC to operate under identical conditions to minimize the complexity of the overall system.

The minimum necessary H_2O excess n_{ex} and thus minimum necessary H_2O/KBH_4 molar FR to avoid by-product precipitation in the hydrolysis reactor in dependence on the reaction temperature and pressure is depicted in Fig. 6 along with the low-temperature PEMFC's typical operating window.
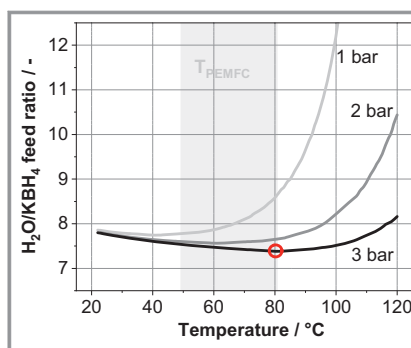

Figure 6. Minimum H_2O/KBH_4 molar feed ratio to avoid by-product crystallization during KBH_4 hydrolysis as a function of temperature and pressure; typical PEMFC operating window indicated in gray and determined, optimized operating conditions highlighted by a circle.

Higher pressures generally have a beneficial effect on the minimum H_2O/KBH_4 FR as the H_2O content in the gas phase and thus the amount of H_2O, which is evaporated from the liquid phase, is decreased with increasing system pressure. In contrast, an optimum system temperature, below which the minimum H_2O/KBH_4 FR is decreasing with increasing temperature and above which the minimum H_2O/KBH_4 FR is increasing with increasing temperature, can be identified for all pressures. This is due to two temperature-dependent phenomena with opposite effects on the necessary H_2O excess n_{ex}: On the one hand, the H_2O vapor pressure is increasing with increasing temperature

leading to increased water evaporation [72], which results in an increased water demand at higher temperatures. On the other hand, higher temperatures result in a slightly higher by-product solubility, as shown in Fig. 2, and thereby help to decrease the necessary amount of H_2O to fully dissolve a certain quantity of KBO_2.

Based on these considerations, an optimum operating temperature and pressure of 80 °C and 3 bar with a corresponding minimum H_2O/KBH_4 FR of 7.4 mol_{H2O} mol_{KBH4}^{-1} (2.5 g_{H2O} g_{KBH4}^{-1}) was identified and employed in all calculations. Under these optimized reaction conditions, the H_2 product stream exits the hydrolysis reactor with a relative humidity of approx. 71 % and could thus be directly fed to the PEMFC without the need for an additional H_2O management system to reduce the risk for FC flooding or dryout of the FC membrane [73].

With only 16 wt %, the solubility of the reactant KBH_4 in H_2O is lower than that of the by-product KBO_2 [23, 24]. Thus, while the by-product stream exiting the hydrolysis reactor is in the form of a solution under the chosen H_2O/KBH_4 FR, the reactant stream entering the reactor is a suspension with a solid particle loading of approx. 15 wt %. From an engineering point of view, this brings along considerable challenges in terms of controlled reactant flow guidance and mixing within the reactor as well as in terms of mechanical catalyst stability and entails the necessity for developing novel catalytic reactor concepts for such multiphase reaction systems. Unlike in the case of $NaBH_4$, limited practical experience of multiphase reactors for the hydrolysis of KBH_4 has, however, been gained and published until now.

3.2 Technical Feasibility of Integrating the Hydrogen Release System on Board of the Model Ship

In order to cater for the model ship's power demand under partial and full load, KBH_4 must be supplied to the hydrolysis system at feed flow rates of 46 g s^{-1} and 113 g s^{-1}, respectively, as can be taken from Fig. 7. The slightly nonlinear relation between the PEMFC's power output and the necessary KBH_4 feed flow rate is due to the considered FC's decreasing efficiency with increasing net power output [52].

Considering that the ship is usually operated at partial load for 95 % of its voyage time [74], an average KBH_4 feed stream of 50 g s^{-1} must be supplied to the on-board H_2 release system. The hydrolysis system's fresh H_2O demand of 113 g s^{-1} under partial, 279 g s^{-1} under full and 121 g s^{-1} under average load can be significantly decreased by recycling the H_2O generated in the FC. In particular, under the previously specified operating conditions, 54 % of the vessel's fresh H_2O demand can be covered through H_2O recirculation. If necessary, a reverse osmosis system such as Pragma Chimica's PRAGMA RO 500 with a permeate throughput of 500 L h^{-1} and an energy consumption of
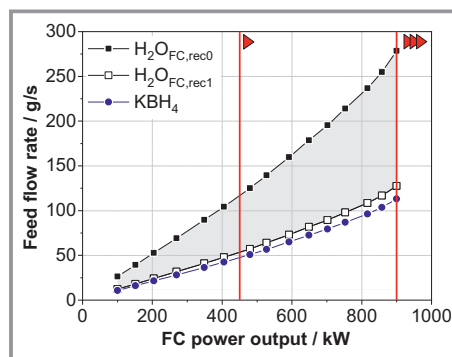

Figure 7. Necessary KBH_4 feed flow rates and external H_2O demand in case 0 % or 100 % of the H_2O generated in the FC is refed to the reactor as a function of the FC's power output; the model ship's power demand under partial and full load of 450 and 900 kW, respectively, is marked by solid lines.

0.55 kW [75] could be employed to purify the freshwater feed stream. This purification system's energy demand accounts for less than 0.2 % of the FC's power output under average load.

In conventional applications, fossil ship fuels are burnt on board of the vessel, which results in an overall weight decrease. By contrast, the use of KBH_4 is characterized by an overall weight increase due to the formation of the 52 % heavier KBO_2 from KBH_4 on the one and the need for on-board storage of considerable amounts of H_2O extracted from the waters surrounding the vessel to avoid by-product crystallization on the other hand. The model ship's overall weight increase under the assumption of a total voyage time of three days without interim loading or unloading can be taken from Fig. 8. Herein, the equipment weight was roughly approximated based on literature data on related technical systems [76] as well as kinetic data [30, 77, 78]. It includes the weight of all major system components, most importantly of the fuel storage tanks, the hydrolysis reactor with gas-liquid separator and the FC stack.
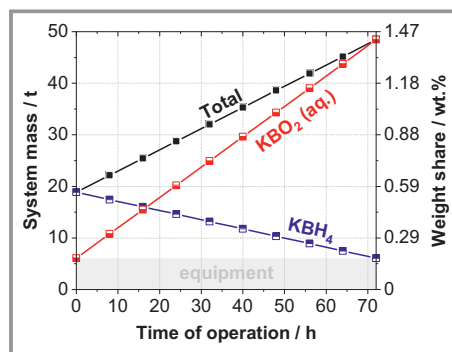

Figure 8. Temporal evolution of the overall H_2 release system weight and corresponding weight share in relation to the model ship's cargo capacity assuming three days of continuous operation; equipment-related system weight indicated in gray.

While the overall mass of the KBH$_4$-based H$_2$ release system is increased by a factor of 2.6 after the vessel's continuous operation of three days, the maximum system weight corresponds to merely 1.4 wt % and the maximum system volume to 0.8 vol % of the model ship's total cargo capacity. The use of KBH$_4$ as energy carrier on board of medium-sized inland-waterway cargo vessels comparable to the model ship employed in the present study is thus deemed feasible from a practical point of view.

3.3 Energetic Evaluation of the Overall Energy Storage Cycle

In comparison to other chemical H$_2$ carriers such as formic acid, dibenzyltoluene or magnesium hydride, from which H$_2$ is released through endothermic processes that require external energy input [15], H$_2$ release from KBH$_4$ through hydrolysis is an exothermic process, which takes place under near-ambient conditions. Hence, this process step requires minimal energy input, which greatly reduces the complexity of the on-board H$_2$ release system.

As can be taken from Fig. 9, a considerable amount of energy is, however, required for the regeneration of the H$_2$-lean storage material in general and for the production of Mg through MgCl$_2$ electrolysis as well as for the solvent (EDA) recovery in particular. The latter are responsible for 41 % and 26 % of the total energy input for KBH$_4$ regeneration, respectively. A reduction of the overall energy demand of up to 13 % with respect to the total energy input and up to 34 % with respect to the energy demand of the core process steps E_{core} can be achieved through heat integration within the individual process steps as indicated in Fig. 4 and 5. While an even more pronounced reduction of the overall energy demand could theoretically be achieved through heat integration not only within but also between the individual subprocesses, such measures were not considered in the present study as they would significantly increase the complexity of the overall process as well as the connected uncertainties.
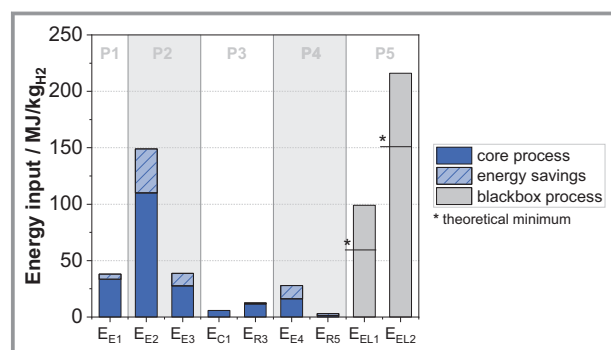
The overall fuel cycle's H$_2$ storage efficiency η_{H2H} defined according to Eq. (6) can be increased from 22 % without to 25 % with heat integration. Under the assumption of H$_2$ production through H$_2$O electrolysis with an efficiency of 60 % and electricity generation in a FC with an efficiency of 50 %, an energy input of 521 MJ is necessary to supply 1 kg of H$_2$ to the FC, which translates into an overall energy storage efficiency η_{E2E} defined according to Eq. (7) of 12 %.

$$\eta_{H2H} = \frac{LHV_{H_2}}{0.5\ LHV_{H_2} + E_{core} + E_{EL2}} \tag{6}$$

$$\eta_{E2E} = \frac{\eta_{FC}\ LHV_{H_2}}{E_{EL1} + E_{core} + E_{EL2}} \tag{7}$$

This relatively high energy demand can mainly be attributed to the need for using MgH$_2$ as auxiliary material in the carrier regeneration step, which results in two connected regeneration cycles instead of merely one recycling step. A more direct route to either regenerate KBH$_4$ without the need for an additional reactant or to reduce the employed auxiliary material's oxide MgO in a more energy-efficient manner is thus highly critical for closing the overall fuel cycle and turning KBH$_4$ into a potential candidate for widely used H$_2$ storage materials. Furthermore, while the herein assumed mechanochemical synthesis of KBH$_4$ through ball milling of KBO$_2$ with MgH$_2$ under ambient conditions has been carried out efficiently on laboratory scale [43], the scale-up of this reactive ball milling process is not straightforward and has not yet been successfully demonstrated [42, 79, 80].

For this reason, several authors proposed regeneration pathways based on the conventional Brown-Schlesinger process for the production of NaBH$_4$ with boric acid as an intermediate product [80, 81], even though the latter is complex and up to now highly energy-intensive [41]. In view of the fact that electricity generation from renewable energy sources will be significantly expanded within the next years [1], the use of electrochemical processes during the spent fuel regeneration can be seen as an interesting option. In this context, the direct reduction of MgO through solid oxide membrane electrolysis could be a promising alternative to the energy-intensive Mg production through electrolysis of MgCl$_2$ considered in the present study [59, 82]. Likewise, the direct electrochemical reduction of the alkali borate could be a promising option [41]. However, only a limited number of studies has been published regarding this topic and until now, no successful implementation of such an electrochemical pathway could be demonstrated [41, 42].

3.4 Comparison with Other, Non-Fossil Energy Storage Materials

As can be taken from Fig. 10a, gravimetric and volumetric energy densities of 7.7 MJ kg$_{tank}^{-1}$ and 5.8 MJ L$_{tank}^{-1}$ can be

Figure 9. Energy demand of the individual KBH$_4$ regeneration steps (P1: spent fuel drying, P2: EDA recovery, P3: MgH$_2$ (de)hydrogenation, P4: Mg evaporation and MgO chlorination, P5: H$_2$O and MgCl$_2$ electrolysis) per kg H$_2$ supplied to the FC.
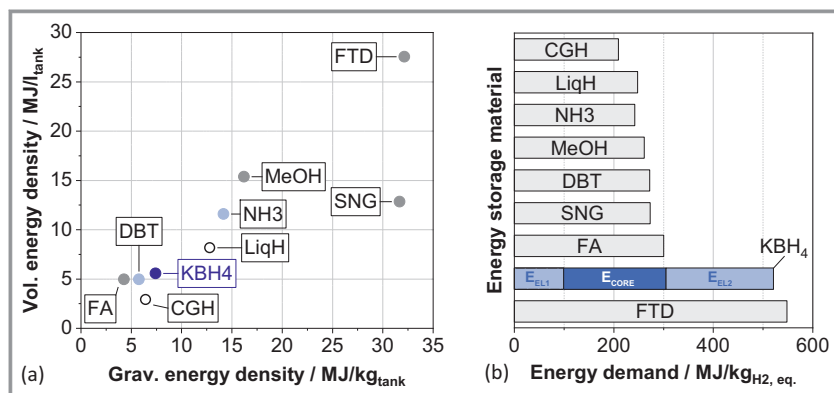
Figure 10. Comparison of KBH$_4$ with other energy carriers in terms of gravimetric and volumetric energy densities (a) and energy demand for producing, storing and eventually releasing 1 kg H$_2$-equivalent (b); values for CGH (compressed H$_2$), LiqH (liquefied H$_2$), FA (formic acid), FTD (Fischer-Tropsch diesel), MeOH (methanol), SNG (synthetic natural gas), DBT (dibenzyltoluene) and NH$_3$ (ammonia) from [15].

achieved with a KBH$_4$-based H$_2$ release system. These values were determined based on the average system mass and overall system volume of a H$_2$ release system suitable for catering for the considered model ship's power demand in case of continuous operation during three days without interim loading or unloading. A qualitative comparison with reference data taken from [15] without further editing shows that KBH$_4$ is superior to the physical storage of H$_2$ at elevated pressures of 700 bar and comparable to other chemical hydrogen carriers such as dibenzyltoluene in terms of energy densities. Similarly, the necessary energy demand for the production, storage and eventual on-board release of 1 kg H$_2$-equivalent is higher but in the same order of magnitude as that of most other, novel energy storage materials, as shown in Fig. 10b.

In comparison with the other non-fossil energy carriers specified in Fig. 10, the use of KBH$_4$ as H$_2$ storage material for shipping applications entails a series of advantages, which are mainly related to the material's facile on-board storage as well as to the nature of the on-board H$_2$ release and power generation. Most importantly, unlike carbon-based energy carriers such as Fischer-Tropsch diesel, synthetic natural gas, methanol and formic acid [15], its on-board use is fully free of the emission of greenhouse gases, particulate matter or other pollutants. Furthermore, KBH$_4$ is a solid material and thus much easier to handle than gaseous or liquefied, toxic ammonia [83]. In contrast to liquid organic hydrogen carriers such as dibenzyltoluene [15], H$_2$ can be released from KBH$_4$ in an exothermal reaction with minimum energy input. Lastly, KBH$_4$ can be stored on board of the ship under near-ambient conditions without the need for excessively high pressures or low temperatures as is the case with the storage of H$_2$ in its physical form through compression or liquefaction [19].

4 Conclusion

A KBH$_4$-based energy storage cycle comprising the H$_2$ release and subsequent electricity generation on board of a ship as well as the onshore regeneration of the H$_2$-lean carrier material was optimized and evaluated on the basis of mass- and energy balances through process simulations in Aspen Plus®.

At an optimum operating temperature and pressure of 80 °C and 3 bar, the on-board H$_2$ release system showed excellent compatibility with the considered low-temperature PEMFC, particularly because the H$_2$ stream entering the FC is already humidified in the hydrolysis reactor, which renders an additional H$_2$O management system unnecessary. A mid-sized inland-waterway cargo vessel with an assumed continuous operation time of three days was employed as model ship to verify the feasibility of using KBH$_4$ as energy carrier in the shipping sector. As the overall weight of the H$_2$ release and power generation system only accounts for 1.4 wt % (0.8 vol %) of the overall cargo capacity, such an installation was deemed feasible.

In the recycling of the H$_2$-lean carrier material, the regeneration of the auxiliary metal Mg through molten salt electrolysis of MgCl$_2$ as well as the recovery of the solvent employed during downstream processing (EDA) were identified as critical process steps and the need for thorough heat integration, which allows for increasing the overall H$_2$ storage efficiency from 22 to 25 %, was underlined.

The system-based gravimetric and volumetric energy densities of 7.7 MJ kg$_{tank}^{-1}$ and 5.8 MJ L$_{tank}^{-1}$, respectively, were found to be comparable with the corresponding values of other, non-fossil energy carriers. However, due to the energy-intensive KBH$_4$ regeneration, the overall energy demand of 521 MJ for releasing 1 kg H$_2$-equivalent on board of the ship was found to be higher than that of most of the other considered energy storage materials and comparable to the energy requirements for producing Fischer-Tropsch diesel.

In conclusion, a high potential can be attributed to KBH$_4$ as energy storage material in the shipping sector based on its ease of handling as well as the facile on-board H$_2$ release and power generation, which is fully free of GHG emissions. However, an efficient pathway for the regeneration of the spent fuel is urgently needed and significant efforts must be undertaken in this field of research, as recyclability is an important prerequisite for the widespread and sustainable use of any chemical energy storage material.

Symbols used

E	[J kg^{-1}]	energy relative to a reference mass
ΔE_{IN}	[J kg^{-1}]	net energy input relative to a reference mass
ΔH_R	[J kg^{-1}]	reaction enthalpy relative to a reference mass
n_{ex}	[–]	water excess
LHV_{H_2}	[J kg^{-1}]	lower heating value of H_2
$\dot{m}_i$	[kg s^{-1}]	mass flow rate of component i
p	[Pa]	pressure
T	[K]	temperature
ΔT	[K]	temperature difference
$w_{i,j}$	[–]	mass fraction of component i in phase j
$x_{i,j}$	[–]	mole fraction of component i in phase j
X	[–]	conversion
η	[–]	efficiency

Sub- and Superscripts

cold	cold stream in a heat exchanger
EDA	ethylenediamine
el	electrical
E2E	energy storage
FC	fuel cell
G	gas
H2H	hydrogen storage
in	inlet
L	liquid
max	maximum
min	minimum
out	outlet
S	solid

Abbreviations

EDA	ethylenediamine
ELECNRTL	electrolyte non-random-two-liquid
FC	fuel cell
FR	feed ratio
GHG	greenhouse gas
IMO	International Maritime Organizations
PEMFC	proton-exchange membrane fuel cell

References

[1] www.consilium.europa.eu/en/eu-climate-change/ (Accessed on October 18, 2021)

[2] https://ec.europa.eu/clima/climate-change/causes-climate-change_en (Accessed on October 18, 2021)

[3] www.ipcc.ch/sr15/ (Accessed on October 18, 2021)

[4] https://webstore.iea.org/co2-emissions-from-fuel-combustion-2020-highlights (Accessed on October 18, 2021)

[5] www.bdl.aero/wp-content/uploads/2021/03/klimaschutzreport2020_final-1.pdf (Accessed on October 18, 2021)

[6] https://ec.europa.eu/clima/eu-action/transport-emissions/reducing-emissions-shipping-sector_en (Accessed on October 18, 2021)

[7] www.imo.org/en/MediaCentre/HotTopics/Pages/Reducing-greenhouse-gas-emissions-from-ships.aspx (Accessed on October 18, 2021).

[8] R. A. Halim, L. K. Kirstein, O. Merk, L. M. Martinez, *Sustainability* **2018**, *10 (7)*, 2243–2272. DOI: https://doi.org/10.3390/su10072243

[9] https://sustainableworldports.org/wp-content/uploads/DNV-GL_2018_Assessment-of-selected-alternative-fuels-and-tech-report.pdf (Accessed on October 18, 2021)

[10] www.imo.org/en/MediaCentre/PressBriefings/Pages/34-IMO-2020-sulphur-limit-.aspx (Accessed on October 18, 2021)

[11] www.thyssenkrupp-uhde-chlorine-engineers.com/en/products/water-electrolysis-hydrogen-production (Accessed on October 18, 2021)

[12] https://energies.airliquide.com/air-liquide-transforms-its-network-germany-connecting-large-electrolyzer-producing-renewable (Accessed on October 18, 2021)

[13] www.e4ships.de/ (Accessed on October 18, 2021)

[14] www.imo.org/en/MediaCentre/Pages/WhatsNew-1636.aspx (Accessed on October 18, 2021)

[15] L. Van Hoecke, L. Laffineur, R. Campe, P. Perreault, S. W. Verbruggen, S. Lenaerts, *Energy Environ. Sci.* **2021**, *14 (2)*, 815–843. DOI: https://doi.org/10.1039/d0ee01545h

[16] P. Gilbert, C. Walsh, M. Traut, U. Kesieme, K. Pazouki, *J. Cleaner Prod.* **2018**, *172*, 855–866. DOI: https://doi.org/10.1016/j.jclepro.2017.10.165

[17] www.energy.gov/eere/fuelcells/hydrogen-storage (Accessed on October 18, 2021)

[18] R. Moradi, K. M. Groth, *Int. J. Hydrogen Energy* **2019**, *44 (23)*, 12254–12269. DOI: https://doi.org/10.1016/j.ijhydene.2019.03.041

[19] U. B. Demirci, *Energy Technol.* **2018**, *6 (3)*, 470–486. DOI: https://doi.org/10.1002/ente.201700486

[20] U. B. Demirci, O. Akdim, P. Miele, *Int. J. Hydrogen Energy* **2009**, *34 (6)*, 2638–2645. DOI: https://doi.org/10.1016/j.ijhydene.2009.01.038

[21] www.energy.gov/eere/fuelcells/downloads/gono-go-recommendation-sodium-borohydride-board-vehicular-hydrogen-storage (Accessed on October 18, 2021)

[22] O. Krol, J. Andrieux, J. J. Counioux, R. Tenu, C. Goutaudier, in *XXXV JEEP – 35th Conf. on Phase Equilibria* (Eds: M. Lomello, S. 1Beauquis, C. Durand, P. Galez), EDP Sciences, Les Ulis **2009**.

[23] A. V. Churikov, K. V. Zapsis, A. V. Ivanishchev, V. O. Sychova, *J. 1Chem. Eng. Data* **2011**, *56 (5)*, 2543–2552. DOI: https://doi.org/10.1021/je200065s

[24] A. V. Churikov, K. V. Zapsis, V. V. Khramkov, M. A. Churikov, I. 1M. Gamayunova, *J. Chem. Eng. Data* **2011**, *56 (3)*, 383–389. DOI: https://doi.org/10.1021/je1007422

[25] A. V. Churikov, K. V. Zapsis, V. V. Khramkov, M. A. Churikov, M. 1P. Smotrov, I. A. Kazarinov, *J. Chem. Eng. Data* **2011**, *56 (1)*, 9–13. DOI: https://doi.org/10.1021/je100576m

[26] O. Sahin, H. Dolas, M. Özdemir, *Int. J. Hydrogen Energy* **2007**, *32 1(13)*, 2330–2336. DOI: https://doi.org/10.1016/j.ijhydene.2006.10.052

[27] I. Dovgaliuk, H. Hagemann, T. Leyssens, M. Devillers, Y. Filinchuk, *Int. J. Hydrogen Energy* **2014**, *39 (34)*, 19603–19608. DOI: https://doi.org/10.1016/j.ijhydene.2014.09.068

[28] D. Kilinc, O. Sahin, *Renewable Energy* **2020**, *161*, 257–264. DOI: https://doi.org/10.1016/j.renene.2020.06.035

[29] D. Xu, H. Wang, Q. Guo, S. Ji, *Fuel Process. Technol.* **2011**, *92 (8)*, 1606–1610. DOI: https://doi.org/10.1016/j.fuproc.2011.04.006

[30] L. Damjanovic, S. Bennici, A. Auroux, *J. Power Sources* **2010**, *195 1(10)*, 3284–3292. DOI: https://doi.org/10.1016/j.jpowsour.2009.11.105

[31] A. Zilberman, G. Nevo-Michrowski, D. Ginzburg, *Patent US20190316735*, **2019**.

[32] A. Silberman, D. Cohen, Y. Duchovny, *Patent US20180265357*, **2018**.

[33] G. Nevo-Michrowski, R. Futerman, *Patent US20190319281*, **2019**.

[34] A. Zilberman, R. Futerman, G. Nevo-Michrowski, *Patent US20190319284*, **2019**.

[35] D. Kilinc., Ö. Sahin., *Int. J. Hydrogen Energy* **2019**, *44 (34)*, 18848–18857. DOI: https://doi.org/10.1016/j.ijhydene.2019.01.229

[36] V. A. Darin, A. F. Neto, A. D. Lanchote Borges, J. Miller, *Main Group Metal Chemistry* **1999**, *22 (8)*, 505. DOI: https://doi.org/10.1515/MGMC.1999.22.8.505

[37] U. B. Demirci, O. Akdim, J. Andrieux, J. Hannauer, R. Chamoun, P. Miele, *Fuel Cells* **2010**, *10 (3)*, 335–350. DOI: https://doi.org/10.1002/fuce.200800171

[38] F. Van Nievelt, *Maritime application of sodium borohydride as an energy carrier*, Master's Thesis, Delft University of Technology **2019**.

[39] http://en.marigreen.eu/feasibility-hydrogen/ (Accessed on February 11, 2022)

[40] S. Xi, X. Wang, D. Wu, S. Hu, S. Zhou, H. Yu, *Front. Chem.* **2020**, *8*, 676. DOI: https://doi.org/10.3389/fchem.2020.00676

[41] H. X. Nunes, D. L. Silva, C. M. Rangel, A. M. F. R. Pinto, *Energies* **2021**, *14 (12)*, 3567. DOI: https://doi.org/10.3390/en14123567

[42] www.osti.gov/biblio/1022594 (Accessed on February 11, 2022)

[43] Z. P. Li, B. H. Liu, N. Morigasaki, S. Suda, *J. Alloys Compd.* **2003**, *354 (1–2)*, 243–247. DOI: https://doi.org/10.1016/S0925-8388(02)01346-4

[44] www.aspentech.com/en/products/engineering/aspen-plus (Accessed on October 18, 2021)

[45] https://webbook.nist.gov/cgi/cbook.cgi?ID=C13709949&Mask=3EFF (Accessed on October 18, 2021)

[46] https://webbook.nist.gov/cgi/cbook.cgi?ID=13762-51-1&Units=SI (Accessed on October 18, 2021)

[47] K. I. M. Al-Malah, *Aspen Plus®: Chemical engineering applications*, John Wiley & Sons, Hoboken, NJ **2016**.

[48] Y. Shang, R. Chen, *SAE Tech. Pap. Ser.* **2011**, *2011-01-1741*. DOI: https://doi.org/10.4271/2011-01-1741

[49] V. I. Simagina, A. M. Ozerova, O. V. Komova, O. V. Netskina, *Catalysts* **2021**, *11 (2)*, 268. DOI: https://doi.org/10.3390/catal11020268

[50] H. Löhn, *Leistungsvergleich von Nieder- und Hochtemperatur-Polymerelektrolytmembran-Brennstoffzellen – Experimentelle Untersuchungen, Modellierung und numerische Simulation*, Ph.D. Thesis, Technische Universität Darmstadt **2010**.

[51] F. Zhu, T. Yamaguchi, K. Yoshida, W. Zhang, H. Liu, Y. Zhou, C. 1Fang, *Analyst* **2020**, *145 (6)*, 2245–2255. DOI: https://doi.org/10.1039/c9an01662g

[52] https://pdf.directindustry.com/pdf/hydrogenics/hypm-hd-180/33492-420321.html (Accessed on October 15, 2021)

[53] L. Laversenne, C. Goutaudier, R. Chiriac, C. Sigala, B. Bonnetot, *J. 1Therm. Anal. Calorim.* **2008**, *94 (3)*, 785–790. DOI: https://doi.org/10.1007/s10973-008-9073-4

[54] Y. Kojima, *R&D Review of Toyota CRDL* **2005**, *40 (2)*, 31–36.

[55] Y. Kojima, T. Haga, *Int. J. Hydrogen Energy* **2003**, *28 (9)*, 989–993. DOI: https://doi.org/10.1016/S0360-3199(02)00173-8

[56] L. Ouyang et al., *J. Power Sources* **2014**, *269*, 768–772. DOI: https://doi.org/10.1016/j.jpowsour.2014.07.074

[57] L. Ouyang, H. Zhong, H.-W. Li, M. Zhu, *Inorganics* **2018**, *6 (1)*, 10. DOI: https://doi.org/10.3390/inorganics6010010

[58] S. Ehrenberger, H. E. Friedrich, *Light Metal Age* **2014**, *72 (1)*, 50–53.

[59] M. Schmitz, *Rohstoffrisikobewertung – Magnesium (Metall)*, DERA Rohstoffinformationen, Deutsche Rohstoffagentur (DERA), Berlin **2019**.

[60] *Essential readings in magnesium technology* (Eds: S. N. Mathaudhu et al.), Springer International Publishers, Cham **2016**.

[61] G. Demirci, *Electrolytic magnesium production using coaxial electrodes*, Ph.D. Thesis, Middle East Technical University **2006**.

[62] F. Liu et al., in *Magnesium Technology 2020* (Eds: J. B. Jordon, V. 1Miller, V. V. Joshi, N. R. Neelameggham), Springer International Publishing, Cham **2020**.

[63] L. H. Prentice, N. Haque, in *Magnesium Technology 2012* (Eds: S. 1N. Mathaudhu, W. H. Sillekens, N. R. Neelameggham, N. 1Hort), John Wiley & Sons, Hoboken, NJ **2012**.

[64] G. J. Kipouros, D. R. Sadoway, in *Advances in Molten Salt Chemistry* (Eds: G. Mamantov, C. B. Mamantov, J. Braunstein), Elsevier, Amsterdam **1987**.

[65] Z. Sun et al., *Nanomaterials* **2020**, *10 (9)*, 1745. DOI: https://doi.org/10.3390/nano10091745

[66] M. Ismail et al., *J. Magnesium Alloys* **2020**, *8 (3)*, 832–840. DOI: https://doi.org/10.1016/j.jma.2020.04.002

[67] Y. Xia, H. D. Lefler, Z. Z. Fang, Y. Zhang, P. Sun, in *Extractive Metallurgy of Titanium* (Eds: Z. Z. Fang, F. H. Froes, Y. Zhang), Elsevier, Amsterdam **2020**.

[68] J. W. Evans, *JOM* **2007**, *59 (2)*, 30–38. DOI: https://doi.org/10.1007/s11837-007-0020-9

[69] https://sendo-shipping.nl/sendo-liner/ (Accessed on September 03, 2021)

[70] https://binnenschifffahrt-online.de/2019/12/schiffstechnik/12175/zwischenbilanz-sendo-liner-erfuellt-die-erwartungen/ (Accessed on September 03, 2021)

[71] www.binnenvaart.eu/motorvrachtschip/49243-sendo-liner.html (Accessed on September 03, 2021)

[72] *VDI-Wärmeatlas* (Eds: P. Stephan et al.), Springer Vieweg, Berlin **2019**.

[73] Z. Chen, D. Ingham, M. Ismail, L. Ma, K. J. Hughes, M. Pourkashanian, *Int. J. Numer. Methods Heat Fluid Flow* **2020**, *30 (4)*, 2077–2097.

[74] www.dst-org.de/wp-content/uploads/2020/05/Fact-Sheet-05_Battery-Electric.pdf (Accessed on September 03, 2021)

[75] www.pragmachimica.it/wp-content/uploads/osmosi.pdf (Accessed on February 11, 2022)

[76] Y. Kojima, K. Suzuki, K. Fukumoto, Y. Kawa, M. Kimbara, H. Nakanishi, S. Matsumoto, *J. Power Sources* **2004**, *125 (1)*, 22–26. DOI: https://doi.org/10.1016/S0378-7753(03)00827-9

[77] J. Andrieux, D. Swierczynski, L. Laversenne, A. Garron, S. Bennici, C. Gooutadier, P. Miele, A. Auroux, B. Bonnetot, *Int. J. Hydrogen Energy* **2009**, *34 (2)*, 938–951. DOI: https://doi.org/10.1016/j.ijhydene.2008.09.102

[78] X. Zhang, J. Zhao, F. Cheng, J. Liang, Z. Tao, J. Chen, *Int. J. 1Hydrogen Energy* **2010**, *35 (15)*, 8363–8369. DOI: https://doi.org/10.1016/j.ijhydene.2009.11.018

[79] T. T. Le, C. Pistidda, J. Puszkiel, C. Milanese, S. Garroni, T. Emmler, G. Capurso, G. Gizer, T. Klassen, M. Dornheim, *Metals* **2019**, *9 (10)*, 1061. DOI: https://doi.org/10.3390/met9101061

[80] C.-H. Liu, B.-H. Chen, D.-J. Lee, J.-R. Ku, F. Tsau, *Ind. Eng. Chem. Res.* **2010**, *49 (20)*, 9864–9869. DOI: https://doi.org/10.1021/ie101309f

[81] C.-H. Liu, B.-H. Chen, *Materials* **2015**, *8 (6)*, 3456–3466. DOI: https://doi.org/10.3390/ma8063456

[82] X. Guan, U. B. Pal, Y. Jiang, S. Su, *J. Sustainable Metall.* **2016**, *2 1(2)*, 152–166. DOI: https://doi.org/10.1007/s40831-016-0044-x

[83] A. Klerke, C. H. Christensen, J. K. Norskov, T. Vegge, *J. Mater. Chem.* **2008**, *18 (20)*, 2304. DOI: https://doi.org/10.1039/b720020j

Performance Evaluation of KBH₄ as Energy Carrier for Shipping Applications

Andrea Düll, Patrick Rohlfs, Olaf Deutschmann, Marion Börnhorst*

Research Article: The performance of potassium borohydride as energy carrier for shipping applications is evaluated on the basis of process simulations in Aspen Plus®. The individual process steps are optimized and storage efficiencies are calculated based on energy balances. An inland-waterway vessel serves as model ship to evaluate the practical feasibility. .... ■